

Terahertz Harmonic Generation from Graphite Pencil Drawings

Atiqa Arshad, Hatice Nur Koyun, Ruslan Salikhov, Michael Gensch, Igor Ilyakov, Alexey Ponomaryov, Gulloo Lal Prajapati, Thales V. A. G. de Oliveira, Kalliopi Mavridou, Jürgen Lindner, Jan-Christoph Deinert, Cumhur Gökhan Ünlü,* and Sergey Kovalev*

The third harmonic generation (THG) of graphite layers on paper substrate upon excitation with intense (up to 100 kV cm^{-1}) narrowband terahertz (THz) pulses is studied. Highest THG efficiencies are comparable with those of chemical vapor deposition-grown single-layer graphene. Samples are hand drawn, using commercially available pencils. The THG response shows high sensitivity regarding the hatching direction relative to the THz polarization orientation. Using Raman spectroscopy, the occurrence of graphene-like structures in the samples is confirmed. The findings demonstrate the feasibility of virtually no-cost and easy-to-fabricate materials for THz nonlinear optics.

1. Introduction

The terahertz (THz) frequency range of the electromagnetic spectrum is attracting considerable attention due to rich opportunities for applications in high-frequency electronics and communications. Over the years, THz technology has found wide use in many fields, such as THz-based electron acceleration,^[1–3] THz spectroscopy with access to low-energy excitations in a matter (rotation of molecules, vibration of crystal lattices, spin precession etc.),^[4–7] nondestructive imaging,^[8,9] and on-chip communication.^[10] At the same time, still there are a number of technological challenges, as (cost) efficient THz sources and detectors are still scarce, despite some significant advances in recent years.^[11] An important component required for various THz technologies is efficient frequency converters and, in particular, THz high harmonic generation (HHG)-based devices. Gapless 2D Dirac materials are a highly promising material class for these applications and have shown very large nonlinear susceptibilities in the THz region and related THz HHG.^[12,13] Harmonic generation up to 7th order has been experimentally demonstrated in single-layer graphene^[12] under 0.3 THz pump. The underlying mechanism of THz harmonic generation is based on the asymmetric dynamics of efficient ultrafast heating and cooling of Dirac fermions during the interaction with picosecond-long oscillating electric fields.^[14] Further Dirac materials that have experimentally shown efficient THz HHG are the 3D Dirac semimetal Cd_3As_2 ^[15,16] and topological insulators.^[17] Additionally, a significant increase in the THz HHG efficiency has been achieved in graphene^[18] and topological insulator-based^[19] metamaterial structures. This increase in sample complexity for higher THz conversion efficiencies is accompanied with an increase in cost and accessibility. The finding that Dirac fermions are the essential prerequisites for efficient THz HHG motivates the research on the possibly simplest and virtually cost-free Dirac system, such as graphite^[20] pencil drawings on paper.

In this article, we study terahertz third harmonic generation (THG) from graphite pencil drawings on paper. We demonstrate that the THz THG yield at 0.5 THz excitation frequency in graphite is comparable to single-layer graphene. The THG in graphite is attributed to the presence of multilayer graphene flakes, which


A. Arshad, I. Ilyakov, A. Ponomaryov, G. L. Prajapati, T. V. A. G. de Oliveira, J.-C. Deinert, S. Kovalev
Institute of Radiation Physics
Helmholtz-Zentrum Dresden-Rossendorf
01328 Dresden, Germany
E-mail: s.kovalev@hzdr.de

H. N. Koyun, R. Salikhov, K. Mavridou, J. Lindner, C. G. Ünlü
Institute of Ion Beam Physics and Materials Research
Helmholtz-Zentrum Dresden-Rossendorf
01328 Dresden, Germany
E-mail: cgokhanunlu@gmail.com

M. Gensch
Institut für Optik und Atomare Physik
Technische Universität Berlin
Straße des 17. Juni 135, 10623 Berlin, Germany

M. Gensch
DLR - Institute of Optical Sensor Systems
Rutherfordstr. 2, 12489 Berlin, Germany

H. N. Koyun, C. G. Ünlü
Department of Biomedical Engineering
Pamukkale University
20160 Denizli, Turkey

 The ORCID identification number(s) for the author(s) of this article can be found under <https://doi.org/10.1002/adpr.202300088>.

© 2023 The Authors. Advanced Photonics Research published by Wiley-VCH GmbH. This is an open access article under the terms of the Creative Commons Attribution License, which permits use, distribution and reproduction in any medium, provided the original work is properly cited.

DOI: 10.1002/adpr.202300088

was confirmed using Raman spectroscopy. Therefore, the feasibility of using easy-to-produce graphite-based structures opens up new possibilities for highly accessible, modifiable, and nearly cost-free THz frequency multipliers, and pencil-drawn THz frequency electronic components.

2. Results and Discussion

Figure 1a shows THz third harmonic electric fields generated in different samples using pump pulses with 0.5 THz central frequency and about 100 kV cm^{-1} maximum peak field. The samples were mounted with the hatching direction in the horizontal plane, that is, perpendicular to the fundamental THz electric field polarization direction. After the samples, two bandpass filters with 1.5 THz central frequency were inserted to completely block the fundamental radiation, and only the THG signal is transmitted. The overall strongest THG signal from a pencil drawing is observed from the *pure graphite* sample (red line in Figure 1a), which was made using a pencil containing the highest available graphite concentration and hardness 9B (Sample A). We used chemical vapor deposition (CVD)-grown graphene as

a reference sample for THz THG, because this type of the THG emitter provides high conversion efficiency and is well characterized in previous publications.^[17] Compared to CVD-grown graphene (0.5% THz THG field conversion efficiency at 100 kV cm^{-1} pump peak fields),^[17] the THG field amplitude is half as large, corresponding to a field conversion efficiency of a few times 10^{-3} at the maximum fundamental field strength available in the experiment. The THz THG field conversion efficiency is determined as a ratio between generated THG peak field and the peak field of the fundamental radiation.^[17] The THz THG electric field from the Graphite Aquarelle sample (Sample B, blue line in Figure 1a) is about 10 times lower compared to the graphene sample, whereas the oil base graphite sample (magenta line in Figure 1a, Sample C) did not show any measurable THz THG signal. Finally, the THz transmission through bare paper exhibited no sign of THz THG, confirming that there is no residual signal at 1.5 THz from the experimental setup. The corresponding Fourier spectra for all samples are shown in Figure 1b.

To get a deeper insight into the THG mechanism especially compared to graphene, we analyzed the THG efficiency as a function of the fundamental beam power. Figure 1c shows the

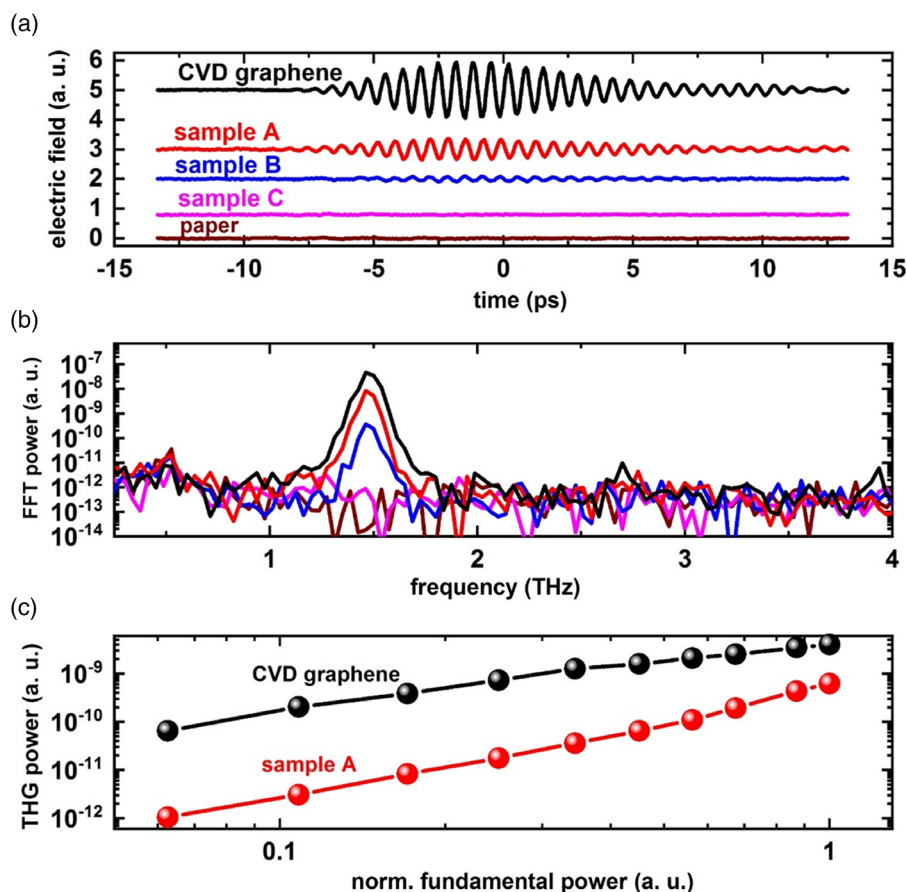


Figure 1. a) Time domain traces of the transmitted fields, as measured using EOS, from single-layer graphene on SiO_2 substrate (CVD graphene), and different graphite pencil drawings on office paper. The hatching direction of the pencil drawings was horizontal, that is, perpendicular to the THz fundamental polarization. The traces are shifted vertically for clarity. b) Corresponding THz THG FFT power spectra of the time-domain signals. c) Logarithmic plot of the power dependence of the THz THG signal in graphene and the pure graphite (sample A). Fits yielded a power law order of 1.45 for graphene and 2.28 for sample A.

comparison of the THG power dependence between sample A and graphene samples. We observe a deviation from cubic power law in both samples, which is in accordance with the saturation effects observed in previous studies on graphene-based samples.^[12,18] More precisely, the graphene sample exhibits a power law dependence with an order of 1.45 ± 0.06 , while the graphite sample (sample A) shows an order of 2.28 ± 0.07 . This indicates that at the moderate-to-high fundamental field strengths used in the experiment graphene is already in the strong saturation regime,^[12] while the *pure graphite* sample does not exhibit such strong saturation behavior. This is particularly apparent for the highest fundamental power values as shown in Figure 1c. Therefore, the THG power in graphite is roughly 100 times lower than that of graphene at low fundamental field strengths, that is, around 10 kV cm^{-1} . However, at the highest available fluence, the power difference is reduced to about a factor of 5. It is therefore conceivable that using even stronger fundamental fields in the MV/cm range, the THG efficiency in graphite potentially could exceed that of graphene. At such high driving field strengths, other THz field-induced phenomena may contribute to the THG response of graphite, potentially leading to the

saturation of the THG efficiency, as observed in graphene. Thus, further research on the THz harmonics response of graphite at MV/cm driving fields is required.

Due to the drawing process using a specific hatching direction, the graphite samples are expected to show a nonisotropic behavior when it comes to their orientation with respect to the THz fundamental field polarization.^[21] Therefore, we measured the THG response for two different sample orientations, 1) with horizontal hatching and 2) vertical hatching, that is, perpendicular and parallel to the vertically polarized incident THz electric field. The time-domain waveforms of fundamental radiation and THG electric fields in sample A are shown in Figure 2a. In this experiment, we utilized 0.3 THz pump pulses and a single bandpass filter with a central frequency of 0.9 THz behind the sample to observe both fundamental and THG signals. To exclusively compare the dependence of THG efficiency on hatching direction, we applied an additional fast Fourier transform (FFT) filter to only pick up THG signals in Figure 2b. We observe an about twice higher value of THz THG field strength from the horizontally hatched orientation as compared to the vertical one. The corresponding FFT power spectra of the raw signals are

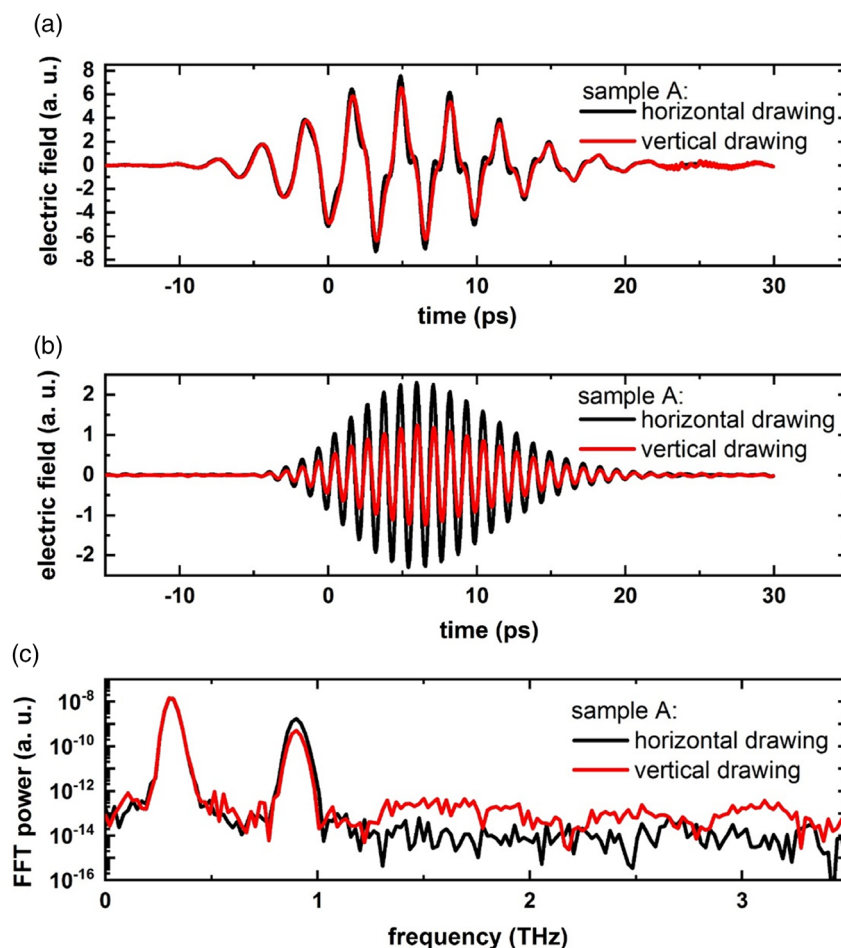


Figure 2. a) Time domain waveforms of fundamental and THG electric fields in sample A for different hatching directions. b) Plot of the THz THG fields in (a) after filtering out the fundamental radiation via an FFT filter. c) Corresponding FFT power spectra of the raw signals in (a).

shown in Figure 2c. We observe the same value for fundamental beam transmission in both hatching directions but a higher value for the THG signal in the horizontally hatched orientation. It is possible that during the process of drawing, where microscopic graphite/graphene flakes are sheared off the pencil tip, dominant channels of high conductivity are formed—similar to a wire grid.^[21] This may lead to a local enhancement of the fundamental field similar as in the aforementioned metamaterials.^[18] At the same time, such a grid structure is not homogeneous over the sample area and thus does not visibly modify the linear THz transmission at fundamental frequency.

For a thorough chemical and structural characterization of the graphite samples, we used Raman spectroscopy under 532 nm laser excitation. The recorded Raman spectra for two different graphite samples and single-layer graphene are presented in Figure 3.

The structural properties of studied carbon materials were deduced from the G, D, and 2D peaks (labeled in Figure 3a) in the Raman spectrum. The Raman spectra of graphene and related materials usually display three main characteristic bands D, G, and 2D, which correspond to 1350, 1580, and 2700 cm^{-1} , respectively.^[22] Graphite consists of stacks of sp^2 bonded graphene sheets.^[23] The chemical bonding between the stacked graphene layers in graphite results in intensity variation of 2D and G peaks. In particular, the 2D band represents the second-order Raman scattering by in-plane transverse optical phonon modes close to the boundary of the Brillouin zone. Therefore, the 2D peak position, its intensity, shape, and width

have a strong relation with the number of atomic layers and the stacking order structure.^[24] Additionally, the G peak represents the in-plane vibration mode of sp^2 -hybridized carbon atoms. Thus, the shape and relative intensity of the 2D and G band provides information of the number of atomic layers and their stacking order. As the number of carbon layers increases, the intensity of the G band increases, and that of the 2D band decreases.^[23] For more than five layers of graphene, the Raman spectrum becomes similar to that of graphite.^[24] This scenario is confirmed by our measurements when comparing the relative intensities of the 2D and G peaks. While the 2D peak intensity is larger than that of the G peak in the Raman spectra of single-layer graphene, both graphite samples show an inverse behavior, indicating the presence of multilayer graphene flakes. Since according to the expectation we observed more than one component within the 2D peak in the different types of graphite samples, we compared the component intensities of 2D peaks to obtain information on the number of the layers.

The 2D peak consists of two dominating components 2D₁ and 2D₂ (high-energy shoulder) in the graphite spectra as shown in Figure 3b. This double-peak structure of the 2D band is due to the splitting of the π -electron dispersion energy, caused by the interaction between the stacked graphene layers in the graphite.^[25] Increasing the number of layers leads to not only a shift in the 2D₂ band, but also to an increase in the intensity of the 2D₂ band, thereby changing the overall shape of the 2D band.^[26] When the intensity of the 2D₂ band is higher than the intensity of the 2D₁ band, the graphite samples are considered much

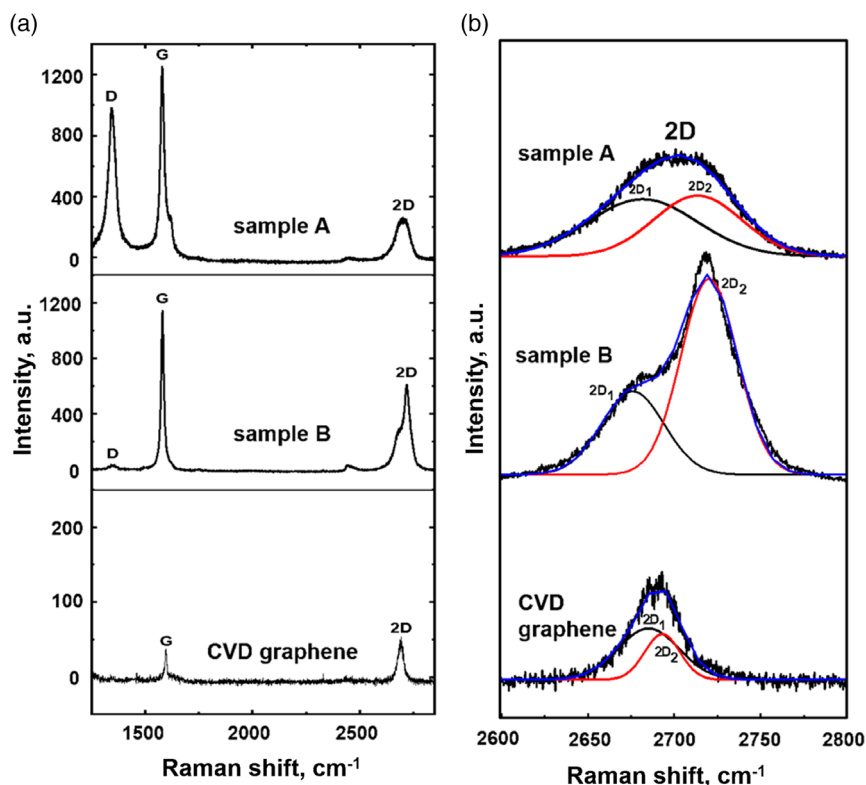


Figure 3. a) Raman spectra of pure graphite (sample A), graphite aquarelle (sample B), and CVD-grown graphene. The spectra are shifted vertically for clarity. b) Zoom-in of the area near the 2D Raman peaks in the corresponding Raman spectra in (a). The blue line is a fit to the experimental curve using the superposition of Gaussian (red lines) and Lorentz (black line) peak profiles.

thicker than 5 layers,^[27] and its properties will have less in common with layered graphene. As shown in Figure 3b, since the 2D₂ band of sample B is more intense than the 2D₁ band, sample B has a much larger number of graphene layers, and thus its properties are less related to graphene. In addition, the roughly matching intensities of the 2D₁ and 2D₂ bands in sample A indicate that the number of layers is low; therefore, it can be concluded that sample A exhibits the characteristics of stacked graphene in contrast to sample B.

The D band originates from the breathing modes of the hexagonal carbon ring structure of graphene and its occurrence is related to defects and disorder of the carbon materials. Any physical or chemical treatments can cause defects in graphite, leading to the appearance of the D band in the Raman spectrum. The intensity ratio of the D and G bands (I_D/I_G) is used to evaluate the amount of structural defects in the carbon materials.^[28] The calculated I_D/I_G ratios of sample B and sample A are 0.03 and 0.79, respectively. The higher I_D/I_G ratio of sample A compared to sample B is indicative of more defective and disordered nature of sample A.

3. Conclusion

We demonstrate efficient terahertz THG using samples made of graphite drawings on paper. The THG efficiency here is comparable with single-layer CVD-grown graphene under 100 kV cm^{-1} pump field strength at a fundamental frequency of 0.5 THz. Remarkably, the THG signal from the graphite/paper samples did not show the harmonic conversion efficiency saturation that is typically present in graphene samples at fields strengths approaching 100 kV cm^{-1} . This might be because the energy relaxation of the excited carriers in the disordered and defective graphene flakes that are present in the graphite/paper sample is significantly faster than in single-layer graphene. It remains to be seen whether at even higher field strengths the THG efficiency in graphite-based samples can even surpass that of single-layer graphene. We showed that the drawing directionality has a strong influence on the THG efficiency, which may enable further functionality by drawing tailored graphite structures, for example, for THz field enhancement or polarization control. We used Raman spectroscopy to characterize the graphene content and structure in our samples. Here, the concentration of stacked graphene-like flakes is supposedly a clear indicator for THG efficiency. Therefore, graphite drawings on paper are a promising playground for fabricating functional and virtually cost-free THz nonlinear optical components. Further, THz harmonic generation might become a powerful tool for nonlinear imaging of buried graphite structures, for example, in paintings, where graphite pencils were used for initial sketching.

4. Experimental Section

Graphite samples were hand drawn with pencils on standard office paper. The pencil was moved across the paper predominantly along one direction with the goal to produce an even graphite coverage without strongly visible hatching. Samples with a number of different coverage thicknesses were produced per pencil and later characterized for THG output. We used a large set of commercially available pencils (Faber-Castell) with different hardness and compositions, namely, Pitt Graphite Pure (sample A), Pitt Graphite Aquarelle (sample B), and Pitt Oil Base (sample C). Samples A, B, and C were drawn with a specific pencil, but each represents

a general type of pencil: Pitt Graphite Pure, Pitt Graphite Aquarelle, and Pitt Oil Base. All samples made with the Pitt Oil Base pencil gave a negligible THz THG signal; the samples made with the Pitt Graphite Pure pencil gave THz THG with a range of amplitudes with $\approx 10\%$ variation; the samples made with the Pitt Graphite Aquarelle pencil showed strong variations in THz THG amplitude, about 90%. Samples A and B were selected as the samples with the highest THz THG efficiency in each group, corresponding to the lowest pencil hardness. To investigate the THz THG anisotropy, different drawing patterns were measured and the anisotropy was reproducible. At the same time, for samples A and B, the THz THG efficiency strongly varied from sample to sample and further systematic studies were needed to understand how to control and improve the THz THG. Besides THz emission characteristics, we characterized the chemical and structural composition of our samples using Raman spectroscopy. As a point of comparison, we examined graphite on paper samples against a single-layer graphene reference sample. The graphene was CVD-grown on a $1 \text{ cm} \times 1 \text{ cm}$ fused silica substrate with a thickness of 0.5 mm.

We performed THz THG experiments using a Ti:Sapphire amplified laser system to generate linearly polarized broadband THz radiation through the tilted pulse front scheme in a LiNbO₃ prism.^[29] To generate narrowband THz radiation, two bandpass filters with a central frequency of 0.3 or 0.5 THz, rejection bandwidth of $>20 \text{ dB}$ in field, and a bandwidth of 20% were placed in the beam path in front of the sample. The filtered THz pulses had about $1 \mu\text{J}$ pulse energy and were focused on the sample to a spot size of $800 \mu\text{m}$ (full width at half maximum (FWHM)). We used one or two bandpass filters with central frequency of 0.9 THz (for 0.3 THz) or 1.5 THz (for 0.5 THz) behind the sample to suppress the transmitted fundamental frequency components while transmitting the third harmonic. The transmitted THz waveform was detected using electro-optic sampling (EOS) in a 2 mm-thick ZnTe crystal. All measurements were performed at ambient conditions.

The Raman measurements were performed using a 532 nm laser in backscattering configuration in a Horiba Scientific LabRAM HR Evolution Raman system. To ensure consistency, the Raman spectra for all samples were recorded under the same experimental conditions within a wavenumber range of $1250\text{--}2850 \text{ cm}^{-1}$.

Acknowledgements

A.A. and H.N.K. contributed equally to this work. This work was supported by the German Research Foundation through the priority program SPP2314 "Integrated TERahertz sySTems Enabling Novel Functionality (INTEREST)" (project IDs GE 3288/1-1).

Open Access funding enabled and organized by Projekt DEAL.

Conflict of Interest

The authors declare no conflict of interest.

Data Availability Statement

The data that support the findings of this study are available from the corresponding author upon reasonable request.

Keywords

Dirac materials, graphite, nonlinear terahertz optics, Raman spectroscopy, terahertz harmonic generation

Received: March 3, 2023

Revised: April 19, 2023

Published online: May 18, 2023

- [1] D. Zhang, M. Fakhari, H. Cankaya, A. L. Calendron, N. H. Matlis, F. X. Kärtner, *Phys. Rev. X* **2020**, *10*, 011067.
- [2] H. Xu, L. Yan, Y. Du, W. Huang, Q. Tian, R. Li, Y. Liang, S. Gu, J. Shi, C. Tang, *Nat. Photonics* **2021**, *15*, 426.
- [3] E. A. Nanni, W. R. Huang, K. H. Hong, K. Ravi, A. Fallahi, G. Moriena, R. J. D. Miller, F. X. Kärtner, *Nat. Commun.* **2015**, *6*, 8486.
- [4] T. Kampfrath, K. Tanaka, K. Nelson, *Nat. Photonics* **2013**, *7*, 680.
- [5] P. Salén, M. Basini, S. Bonetti, J. Hebling, M. Krasilnikov, A. Y. Nikitin, G. Shamuilov, Z. Tibai, V. Zhaunerchyk, Y. Goryashko, *Phys. Rep.* **2019**, *836–837*, 1.
- [6] T. Nörenberg, G. A. Pérez, M. Obst, L. Wehmeier, F. Hempel, J. M. Klopff, A. Y. Nikitin, S. C. Kehr, L. M. Eng, P. Alonso-González, T. V. A. G. de Oliveira, *ACS Nano* **2022**, *16*, 20174.
- [7] T. V. A. G. de Oliveira, T. Nörenberg, G. A. Pérez, L. Wehmeier, J. Taboada-Gutiérrez, M. Obst, F. Hempel, E. J. H. Lee, J. M. Klopff, I. Errea, A. Y. Nikitin, S. C. Kehr, P. Alonso-González, L. M. Eng, *Adv. Mater.* **2021**, *33*, 2005777.
- [8] R. I. Stantchev, X. Yu, T. Blu, E. P. MacPherson, *Nat. Commun.* **2020**, *11*, 2535.
- [9] D. M. Mittleman, *Opt. Express* **2018**, *26*, 9417.
- [10] Y. Yang, Y. Yamagami, X. Yu, P. Pitchappa, J. Webber, B. Zhang, M. Fujita, T. Nagatsuma, R. Singh, *Nat. Photonics* **2020**, *14*, 446.
- [11] T. Seifert, S. Jaiswal, U. Martens, J. Hannegan, L. Braun, P. Maldonado, F. Freimuth, A. Kronenberg, J. Henrizi, I. Radu, E. Beaurepaire, Y. Mokrousov, P. M. Oppeneer, M. Jourdan, G. Jakob, D. Turchinovich, L. M. Hayden, M. Wolf, M. Münzenberg, M. Kläui, T. Kampfrath, *Nat. Photonics* **2016**, *10*, 483.
- [12] H. Hafez, S. Kovalev, J.-C. Deinert, Z. Mics, B. Green, N. Awari, M. Chen, S. Germanskiy, U. Lehnert, J. Teichert, Z. Wang, K.-J. Tielrooij, Z. Liu, Z. Chen, A. Narita, K. Müllen, M. Bonn, M. Gensch, D. Turchinovich, *Nature* **2018**, *561*, 507.
- [13] H. Hafez, S. Kovalev, K. Tielrooij, M. Bonn, M. Gensch, D. Turchinovich, *Adv. Opt. Mater.* **2020**, *8*, 1900771.
- [14] Z. Mics, K. Tielrooij, K. Parvez, S. Jensen, I. Ivanov, X. Feng, K. Müllen, M. Bonn, D. Turchinovich, *Nat. Commun.* **2015**, *6*, 7655.
- [15] B. Cheng, N. Kanda, T. N. Ikeda, T. Matsuda, P. Xia, T. Schumann, S. Stemmer, J. Itatani, N. P. Armitage, R. Matsunaga, *Phys. Rev. Lett.* **2020**, *124*, 117402.
- [16] S. Kovalev, R. M. A. Dantas, S. Germanskiy, J.-C. Deinert, B. Green, I. Ilyakov, N. Awari, M. Chen, M. Bawatna, J. Ling, F. Xiu, P. H. M. V. Loosdrecht, P. Surówka, T. Oka, Z. Wang, *Nat. Commun.* **2020**, *11*, 2451.
- [17] S. Kovalev, K. Tielrooij, J.-C. Deinert, I. Ilyakov, N. Awari, M. Chen, A. Ponomaryov, M. Bawatna, T. V. A. G. de Oliveria, L. M. Eng, K. A. Kuznetsov, D. A. Safaronenkov, G. K. Kitaeva, P. I. Kuznetsov, H. A. Hafez, D. Turchinovich, M. Gensch, *npj Quantum Mater.* **2021**, *6*, 84.
- [18] J.-C. Deinert, D. A. Iranzo, R. Pérez, X. Jia, H. Hafez, I. Ilyakov, N. Awari, M. Chen, M. Bawatna, A. Ponomaryov, S. Germanskiy, M. Bonn, F. H. L. Koppens, D. Turchinovich, M. Gensch, S. Kovalev, K. Tielrooij, *ACS Nano* **2021**, *15*, 1145.
- [19] K. Tielrooij, A. Principi, D. S. Reig, A. Block, S. Varghese, S. Schreyeck, K. Brunner, G. Karczewski, I. Ilyakov, O. Ponomaryov, T. V. A. G. de Oliveria, M. Chen, J.-C. Deinert, C. G. Carbonell, S. O. Valenzuela, L. W. Molenkamp, T. Kiessling, G. V. Astokhov, S. Kovalev, *Light Sci. Appl.* **2022**, *11*, 315.
- [20] S. Y. Zhou, G.-H. Gweon, J. Graf, A. V. Fedorov, C. D. Spataru, R. D. Diehl, Y. Kopelevich, D.-H. Lee, S. G. Louie, A. Lanzara, *Nat. Phys.* **2006**, *2*, 595.
- [21] M. P. M. Colleoni, B. Vidal, *Opt. Express* **2014**, *22*, 30156.
- [22] B. Tang, H. Guoxin, H. Gao, *Appl. Spectrosc. Rev.* **2010**, *45*, 369.
- [23] A. C. Ferrari, *Solid State Commun.* **2007**, *143*, 47.
- [24] A. C. Ferrari, J. C. Meyer, V. Scardaci, C. Casiraghi, M. Lazzeri, F. Mauri, S. Piscanec, D. Jiang, K. S. Novoselov, S. Roth, A. K. Geim, *Phys. Rev. Lett.* **2006**, *97*, 187401.
- [25] A. Kaniyoor, S. Ramaprabhu, *AIP Adv.* **2012**, *2*, 032183.
- [26] A. Das, B. Chakraborty, A. K. Sood, *Bull. Mater. Sci.* **2008**, *31*, 579.
- [27] A. C. Ferrari, D. M. Basko, *Nat. Nanotechnol.* **2013**, *8*, 235.
- [28] D. Liu, Y. Dong, Y. Liu, N. Ma, G. Sui, *Front. Mater.* **2019**, *6*, 235.
- [29] K.-L. Yeh, M. C. Hoffmann, J. Hebling, K. A. Nelson, *Appl. Phys. Lett.* **2007**, *90*, 171121.